SQUID Microscope read-out on a Josephson junction array

Cinzia De Leo and Giacomo Rotoli[§]

Università di L'Aquila, Dipartimento di Energetica and [§] I.N.F.M.,

Località Monteluco I67041, L'Aquila, ITALY

Abstract—LTC Josephson Junction Arrays (JJA) have recently gained interest as model for the study of magnetization in superconductor materials. The presence of Paramagnetic Meissner Effect in such devices when field cooled make them an excellent candidate to discriminate between the different explanations given for such phenomenon. On the other hand the understanding of the JJA physics is not simple due to the interplay between the non-linear behavior of Josephson devices and the mutual induction effects in large JJA. The use of a SQUID Microscope (SSM) to catch the magnetic image of the array is a distinctive feature of the experiment. So a study of SQUID read-out based on the actual JJA magnetic behavior is needed to have a correct picture of what is going on. In this contribution, using a simple way to reconstruct the complex array far-field viewed by the SQUID, we study how the flux read-out is dependent on array resolution, distance, tilting, and noise for the typical situations in which arrays are found.

I.INTRODUCTION

A significant achievement of last years research in the field of magnetic images was the use of SQUID microscope (SSM) for the analysis of local magnetization in HTC superconductors [1],[2]. Among the most interesting experimental results is the Paramagnetic Meissner Effect (PME) that was found first in HTC materials [3] and then in LTC structures [4]. This raising a puzzling question about the role of d-wave superconductivity in the paramagnetic HTC samples [5]. On the other hand many studies have shown the importance of the use of LTC Josephson junction arrays for the modeling of the granular superconductors [6]-[8]. In this paper we show, by means of full mutual inductance simulations of a two-dimensional LTC Josephson Junction Array (JJA), how the read-out of the SSM can be traced back to the sample magnetic response. Here we concentrate on data analysis showing the effects of resolution, sample distance and tilting. The consequences of PME dominance in JJA have been treated elsewhere [9].

II. JJA MODEL

We simulate an array of NxN meshes each carrying four Josephson junctions. The equations describing the array in vector notation read as [9]:

$$\frac{\beta_L}{2\pi}\sin\vec{\varphi}+\sqrt{\frac{\beta_L}{\beta_C}}\dot{\vec{\varphi}}+\ddot{\vec{\varphi}}=\hat{K}\hat{L}^{-1}\vec{m} \tag{1}$$

here $\vec{\varphi}$ represents a vector containing the phases of all the junctions in the array; $\beta_L = 2\pi L I_0/\Phi_0$ with I_0 the critical current of junctions, L the mesh self-inductance and Φ_0 the flux quantum; $\beta_C = 2\pi C I_0/G^2\Phi_0$ is the Stewart-McCumber parameter, with C the junction capacitance and G the quasi-particle conductance; $\hat{K}$ is a matrix depending on array geometry and $\hat{L}$ is the full mutual inductance matrix of the array, i.e., the matrix containing mutual inductances of any mesh of the array with all the other mesh [6]. The vector $\vec{m}$ represents the mesh magnetization and its expression is:

$$\vec{m} = \frac{\vec{\phi}_{tot}}{\Phi_0} - \frac{\vec{\phi}_{extt}}{\Phi_0} = \frac{1}{2\pi}\left(\hat{M}\vec{\varphi} + 2\pi\vec{n} - 2\pi\vec{f}\right) \tag{2}$$

where $\vec{M}$ is an integer matrix performing (oriented) summing up the phases of each mesh; $\vec{n}$ is an integer vector and $\vec{f}$ is the normalized external flux in each mesh which modulus is the so-called frustation $f=\Phi/\Phi_0$. It is worth to note that (2) represents nothing else than flux quantization with $\vec{n}$ the quantum number. Here quantum numbers are used to introduce noise in the system choosing them randomly distributed (see discussion below). We ignore the spread in critical currents of the junctions because no qualitative effect is connected with it: spread in critical currents simply change slightly the values of mean magnetization over the whole array, changing randomly the magnetization of some meshes, but *do not change* the observed diamagnetism or paramagnetism and the general aspect of the simulated magnetic images obtained below. To simulate field cooling we integrate numerically the system (1) starting by a given frustation *f* and increasing β_L in step until its final value. According to (1) this means that screening supercurrents become different from zero. After a proper time interval the phases are collected when all the transitory effects in the dynamical terms of (1) wane out. Details of the integration routine can be found in [10] where also a slightly different derivation of array equations and the expression of mutual inductance matrix are given. The prevailing response of

N>5 array to field cooling procedure is found to be paramagnetic just for small values of frustation, e.g., for f>3 for arrays with N=10, only for small values and in some interval, e.g., k<f<k+1/2 with k=0,1,2 for N=10, the array is diamagnetic. This behavior can be justified by two main reasons: i) a single mesh with four Josephson junctions shows paramagnetism for any values of frustation such that k+1/2<f<k+1 with k integer; ii) mutual inductances and boundary effects tend to favor a paramagnetic response in the center of the array [9]. To compare our results with that in literature here we choose β_L=30 and β_C =65 as in ref.s [5],[9]. We use a small 10x10 JJA in order to have compact figures and shown a complete series of images for each value of f. Larger JJA's are treated in [9]-[11] with similar results in terms of diamagnetic/paramagnetic response. The effect of variation of β_L is shown in [11]. We note that for the value of β_L used here arrays are found to show paramagnetism just from about N=5 [9].

III. FAR-FIELD COSTRUCTION

Once (1) was integrated, and the phase vector determined, the JJA magnetization can be easily generated using Eq.(2). But this vector represents magnetization of meshes on the array plane, i.e., a mean value evaluated at *zero* distance from the array. Naturally the SQUID read-out is sampled not on the array plane but at a given distance z. Moreover the value of magnetization, which here is essentially a flux, is dependent on the SQUID resolution, here represented by an "equivalent" input loop of area S. So to have a faithful read-out is necessary calculate the JJA far-field. Having all current in the branches of the array the construction of the magnetic far field of the array is made by superposition. For each branch we use the expression [12]:

$$\vec{B} = \frac{\mu_0 I_b}{4\pi r}\left[\sin\theta_1 \pm \sin\theta_2\right]\hat{u} \tag{3}$$

where I_b is the branch current; θ_1 and θ_2 are the view angles of the branch and r the distance from the observation point in which the field is calculated; $\hat{u}$ is an unit length vector along the circumference in the plane orthogonal to the branch passing for the observation point (cf. Fig.1a). The sign plus/minus between the sin in Eq.(3) depend on the position of the observation point: if point in the space slice containing the branch and limited by two orthogonal planes placed at the ends of branch then the sign is plus, otherwise it is minus. After the total field is known it become possible evaluate the flux in a given loop of area S which center is placed at distance z with a tilting angle α over the array (cf. Fig.1b). This flux is what is viewed by the SSM, so moving the loop using a step procedure [5] will generate a magnetic image of the array. Thus the image depends on S, z and α, beyond its dependence on the array field. Furthermore it can also depends on the step procedure used for obtaining image (see below). In generating magnetic images flux is considered diamagnetic when its sign is opposite to the given external flux and paramagnetic when the sign is the same. Naturally when we sample the flux over the array some of flux lines can be lost, so the resulting mean magnetization is generally different from zero distance magnetization evaluated using (2). In all simulated JJA field cooling procedures (cf. also [9,11]) however the sign of far-field mean magnetization was always the same of the sign of zero distance mean magnetization evaluated by (2) (except in the special case of f=k+1/2 where magnetization is very small and errors deriving from far-field procedure can be large). So both qualitatively, by looking directly to the magnetic images, and quantitatively, by looking to the mean magnetization, the gross response of the array, i.e., the paramagnetic or diamagnetic behavior, was always correctly determined. On the other hand we note that the magnetic field of a randomly magnetized array is very complex and not intuitively similar to a simple sum of magnetic moments of the mesh loops. For example above a branch the z-component of the magnetic field can be very near to zero if the next-neighbor branch interfere destructively (as happen if they support equal sign currents

roughly of the same modulus). This can imply that part of the flux lines close on itself before to reach the read-out loop. So the values of the far-field mean magnetization tend to be smaller than zero distance magnetization. Another important effect is the related to the tilt angle α. A systematic tilt angle always cause some read-out error because some small component of the field can reverse its sign in the magnetization. These errors are evaluated below. Tilt angles also give illustration to the above described properties of the array magnetic field permitting to sample flux in directions different from z. In principle this can used to give a more complete information on the magnetic field of the array.

IV. SIMULATED SSM READ-OUT

In Fig.2 we shown the flux sampled at a distance z over a 10x10 JJA with a frustation f=1.2. For such value of frustation the array is diamagnetic (cf.[9]). At a fixed distance z the parameter controlling the image resolution is the SQUID "equivalent" input loop area S. The zero distance magnetization evaluated by (2) is shown in Fig.2d, other images can be compared with this. In Fig.2b we shown an high resolution magnetic image of the array with S equal to a 1/100 of the mesh area. In Fig.2c an intermediate resolution is shown sampling asymmetrically one of the coordinates as in [5], i.e., stepping at about 1/10 of mesh in one direction and of 1 mesh in the other. Here S is equal to the area of one mesh but this give an image with more details, so resolution is slightly better (roughly equal to 1/10 of the mesh area). Fig.2c is interesting because though it represents magnetization over a 10x10 array, it compare locally very well with magnetic images reported in [5] over much larger arrays. In Fig.2d the lowest resolution is shown: S coincide with mesh area. We note that diamagnetic low frustation response of the array is signaled by a large number of sampled diamagnetic fluxes, i.e., array meshes appear mostly diamagnetic screening the external flux as in the Meissner standard response. Only few meshes are paramagnetic: though their magnetization is stronger, they

cannot change the mean magnetization of the array that remains diamagnetic. We note that the solution for the single mesh is diamagnetic here.

In Fig.3 we report the magnetic images of the same array with a different frustation f=4.8. The array shows a strong paramagnetic response. Again zero distance magnetization is reported in Fig.3a. In Fig.3b we show the higher resolution with S=1/100 of mesh. Fig.3c is the asymmetric sampling described above, and finally Fig.3d is the low-resolution image with S=1. Here the array response is practically reversed respect to diamagnetic case of Fig.2. In all meshes the paramagnetism is dominant with the exceptions of few diamagnetic meshes. The resulting mean magnetization is positive though diamagnetic meshes show the largest values of magnetization. We note that for f=4.8 the single mesh solution is also paramagnetic.

Though the first two cases shown that array magnetization is related to the single mesh case this is not longer true for larger values of frustation. An example of this behavior is shown in Fig.4 where again the same arrays is shown with f=12.2. Here as is evident from Fig.4a, that is reporting the zero distance magnetization, the background of the array is diamagnetic, but the number of paramagnetic meshes is increased unbalancing the mean magnetization toward paramagnetism. This is viewed by SSM mapping the strongly paramagnetic meshes by superposition of far-fields, over more dispersed structures. Thus the general far-field appearance of the array, here reported for the same resolutions of previous cases, given in Fig.4b, 4c and 4d is similar to that of Fig.3 rather than Fig.2.

In Fig.5 is shown the effect of varying the sampling distance in term of histogram of mesh magnetization for f=1.2. The two peaks in Fig.5a are the diamagnetic and paramagnetic zero distance mesh magnetization (the values are essentially the same of the single mesh with a small dispersion). According to Fig.2 the number of diamagnetic mesh is prevailing. In Fig.5b, c and d the same histogram is evaluated with a resolution of S=1/100 mesh varying the distance

z from 1/10 of mesh until 1 mesh. With the increase of the distance the peaks merge giving a single histogram. Smaller distance, though difficult to reach for actual SSMs, gives an accurate measurement of zero distance magnetization. The mean magnetization, i.e., the average value of m over the array, at z=0 is –0.0527, this value will decrease to –0.0148 when the mean is evaluated at the maximum distance z=1. This variation is due to the fact that many flux lines close before they reach the z=1 quote as we explain above, moreover some flux escape by divergence of flux lines by the array boundaries.

For f=4.8 the dependences on the distance z, which are shown in Fig.6, are very similar except for the inversion of the position of the peaks that is consequence of paramagnetic meshes prevalence. Mean magnetization will vary from 0.0421 at z=0 to 0.0133 at z=1. Finally in Fig.7 we report the histograms for the case f=12.2. They appears similar to that of Fig.5, with the exception that how is evident from Fig.7a the number of paramagnetic meshes is increased. Mean magnetization will be positive in this case accordingly to the image paramagnetic appearance, it will range from 0.0182 at z=0 to 0.0065 at z=1.

In simulations particular importance to obtain SSM simulated images comparable with experiments is to be ascribed to the random choice of the vector of quantum numbers $\vec{n}$. The reason for this procedure is the following: at the beginning of the simulation Josephson energy is very small so thermal noise is dominant and can put random phase-slips in the array, these corresponds to give a random distribution of quantum numbers n over the array. Next this distribution is frozen when the Josephson barriers overcomes the thermal noise. The principal characteristic of noise free image, i.e., with n=0 for each mesh of the array, is its symmetry: in diamagnetic arrays paramagnetic meshes dispose symmetrically over the background of diamagnetic meshes and the opposite happens in paramagnetic arrays. Anyway we note that also this very improbable distribution give roughly the same mean magnetization of the

noised simulations. The variation of the mean magnetization for the change of distribution of quantum numbers was evaluated to be roughly of 2% at least for the number of statistical realizations we have simulated which here is of 10-12 for each frustation value. The result is the same for larger array [9]-[11], though due to long CPU times the number of realization is roughly halved.

In Fig.8 is reported the tilting angle effect showing how the normalized mean magnetization change in function of the tilt angles for two values of z and the three frustrations reported above. Naturally the particular statistical realization of quantum number distribution is responsible of the position of the maximum which depends on which mean direction the flux in the SQUID loop is maximum so this is different for the three frustation shown in the figure. From Fig.8 the mean magnetization can vary between 2% and 10% for about 10 degree of tilt. Smallest frustation f=1.2 give the most symmetric curve and so smallest errors. This give an idea of the errors associated to the tilt. We note that the changing of z have a limited effect in this case also if in the z=0.1 for f=12.2 the maximum is more near to the zero tilt which is the ideal situation. We suggest that tilt angles can be in principle used to reconstruct the 3D field locally: measurements at two different tilt angles can give an estimate of the two field components in the plane orthogonal to the rotation and so a 3D reconstruction of the magnetic field over the array.

V. CONCLUSION

We have shown by means of numerical simulations of field cooling experiments on LTC-JJA how magnetic images of the array taken by a SSM are influenced by resolution, distance and tilting of the input SQUID loop. Beyond this a number of improvements and further studies can be suggested. Among these the study of paramagnetic response via

magnetic images of more complex situation, e.g., disordered JJA or arrays containing the so-called π-junctions, is the most promising.

ACKNOWLEDGMENT

We thank warmly P.Barbara, A.P.Nielsen and C.J.Lobb for useful discussions and suggestions. This research was supported by Italian MURST Cofin2000 Project *Dynamics and Thermodynamics of vortex structures in supeconducting tunneling*.

REFERENCES

[1] F.Tafuri and J.R.Kirtley, Phys.Rev.B**62**, 13934, 2000.

[2] J.R.Kirtley, A.C.Mota, M.Sigrist and T.M.Rice, J.Phys.: Cond.Mat.**10**, L97, 1998.

[3] W.Braunisch, N.Knauf, S.Neuhausen, A.Grutz, A.Koch, B.Roden, D.Khomskii and D.Wohlleben, Phys.Rev.Lett.**68**, 1908, 1992.

[4] D.J.Thompson, M.S.M.Minhaj, L.E.Wenger and J.T.Chen, Phys.Rev.Lett.**75**, 529, 1995.

[5] A.P.Nielsen, A.B.Cawthorne, P.Barbara, F.C.Wellstood, C.J.Lobb, R.S.Newrock and M.G.Forrester, Phys.Rev.B**62**, 14380, 2000.

[6] R.Fehrenbecher, V.B.Geshkenbein and G.Blatter, Phys.Rev.B**45**, 5450, 1992.

[7] A.Majhofer, T.Wolf and W.Dieterich, Phys.Rev.B**44**, 9634, 1991.

[8] D.Domìnguez and J.V.Josè, Phys.Rev.B**53**, 11692, 1996.

[9] C. De Leo, G.Rotoli, A.P.Nielsen, P.Barbara and C.J.Lobb, submitted to Phys.Rev.B, March 2001.

[10] A.Petraglia, G.Filatrella and G.Rotoli, Eur.J.Phys.B**12**, 23, 1999.

[11] C.De Leo and G.Rotoli, submitted to Studies in Superconductivity, ed. V.J.Narlikar, June 2001, see preprint at http://www.ing.univaq.it/energeti/Fisica/supgru.htm

[12] E.Durand, *Magnètostatique*, Masson, Paris 1953.

FIGURE CAPTIONS

Fig.1. The far-field construction is shown in (a). The procedure for generate the magnetic images is reported in (b), here the loop have arbitrary area S, tilt angle α and distance z from the JJA.

Fig.2. Simulated magnetic images of a 10x10 JJA with β_L=30, *f*=1.2 and z=1 mesh. a) the zero distance magnetization evaluated by (2); b) S=1/100 of mesh; c) asymmetric sampling 10 point per mesh in one direction corresponding to about 1/10 of mesh; d) S=1 mesh.

Fig.3. Simulated magnetic images of a 10x10 JJA with β_L=30, *f*=4.8 and z=1 mesh. a) the zero distance magnetization evaluated by (2); b) S=1/100 of mesh; c) asymmetric sampling 10 point per mesh in one direction corresponding to about 1/10 of mesh; d) S=1 mesh.

Fig.4. Simulated magnetic images of a 10x10 JJA with β_L=30, *f*=12.2 and z=1 mesh. a) the zero distance magnetization evaluated by (2); b) S=1/100 of mesh; c) asymmetric sampling 10 point per mesh in one direction corresponding to about 1/10 of mesh; d) S=1 mesh.

Fig.5. Histograms of mesh magnetization for a 10x10 JJA with β_L=30, *f*=1.2 and S=1/100. a) the zero distance magnetization histogram; b) z=0.1 mesh; c) z=0.5 mesh; d) z=1 mesh.

Fig.6. Histograms of mesh magnetization for a 10x10 JJA with β_L=30, *f*=4.8 and S=1/100. a) the zero distance magnetization histogram; b) z=0.1 mesh; c) z=0.5 mesh; d) z=1 mesh.

Fig.7. Histograms of mesh magnetization for a 10x10 JJA with β_L=30, *f*=12.2 and S=1/100. a) the zero distance magnetization histogram; b) z=0.1 mesh; c) z=0.5 mesh; d) z=1 mesh.

Fig.8. Tilting angle effect on a sampled flux on a 10x10 JJA with β_L=30, *f*=12.2, with d=1 mesh and S=1 mesh: (a) z=0.1, *f*=1.2 triangles, *f*=4.8 circles, *f*=12.2 squares; (b) z=1 , *f*=1.2 triangles, *f*=4.8 circles, *f*=12.2 squares.

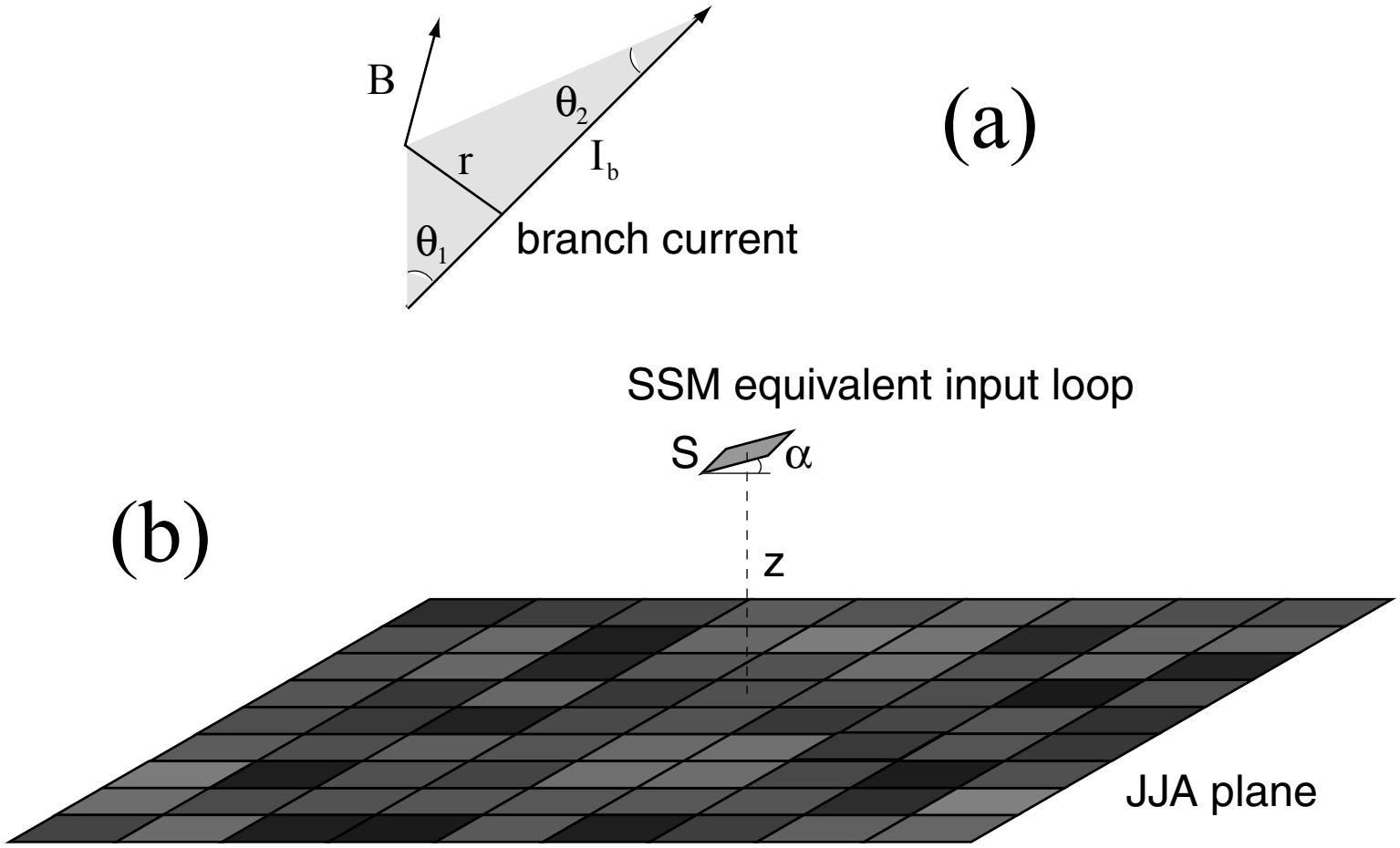
B
θ2
r
Ib
θ1
branch current
(a)
SSM equivalent input loop
S
α
(b)
z
JJA plane

Fig.1

Fig.2

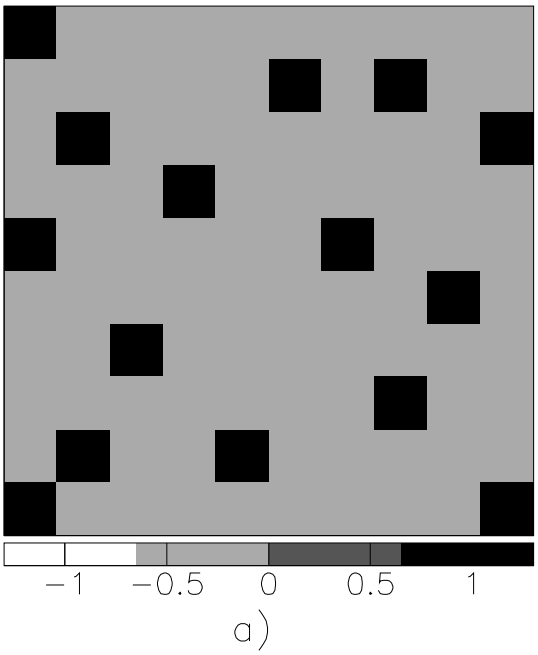

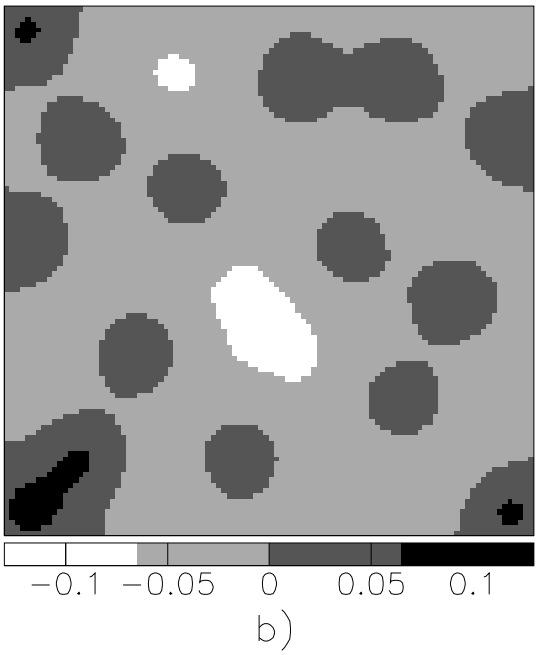

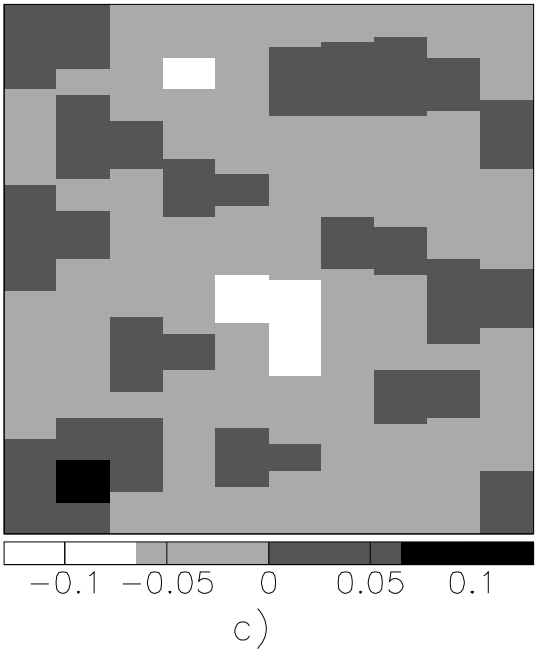

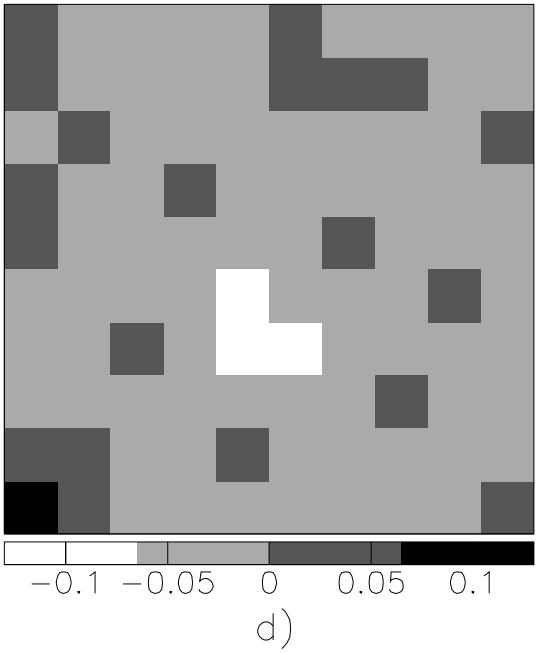

Fig.3

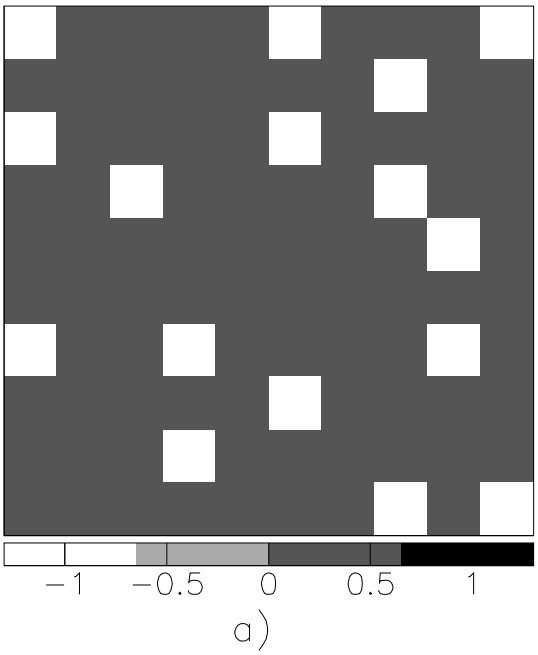

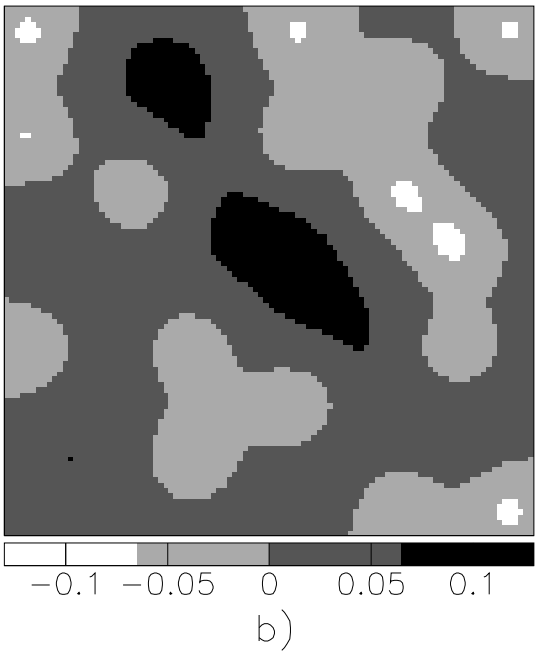

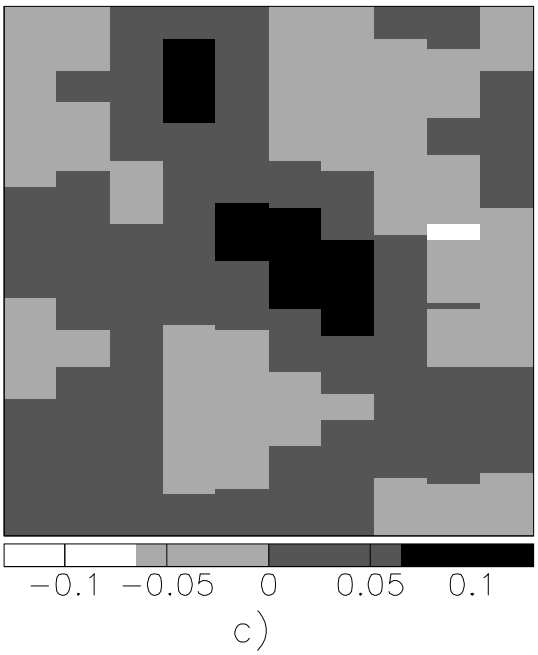

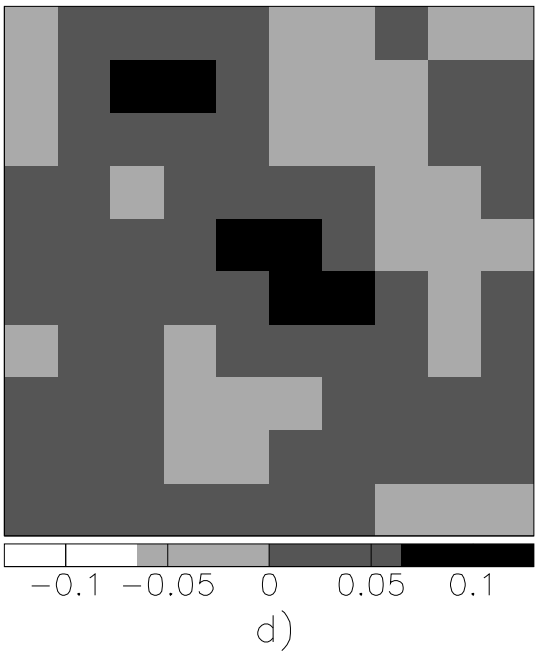

Fig.4

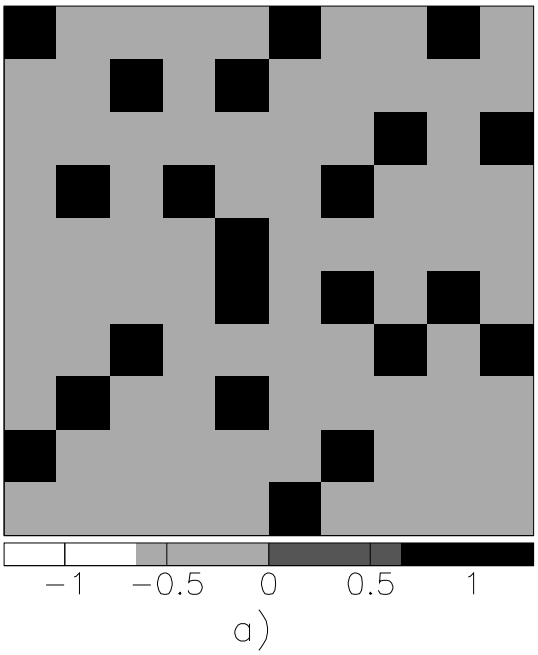

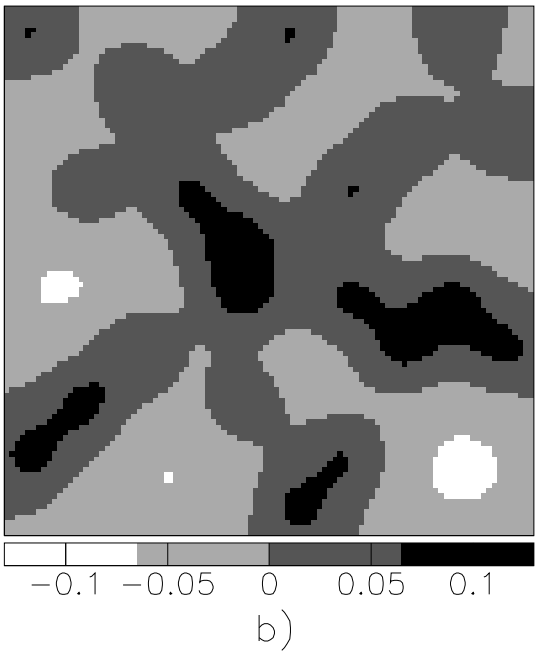

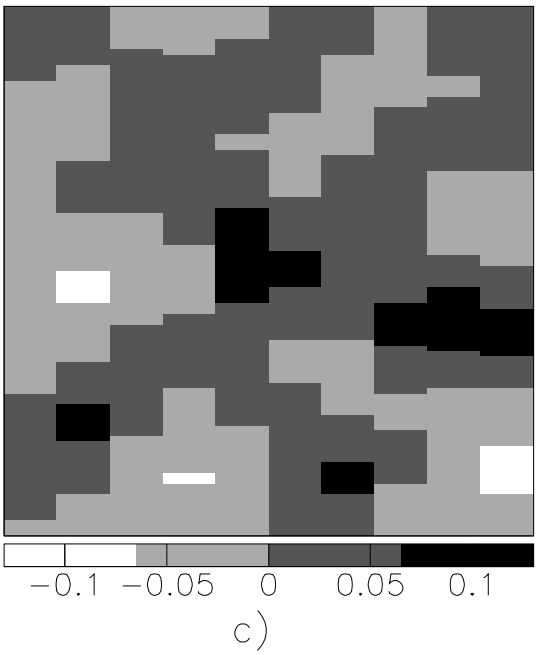

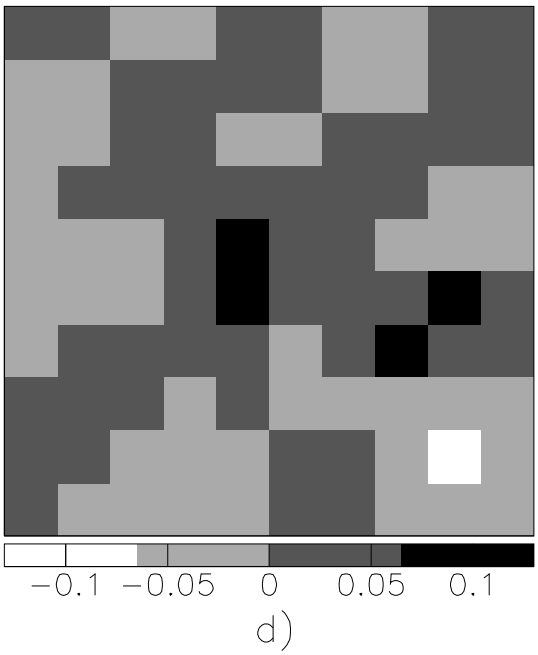

Fig.5

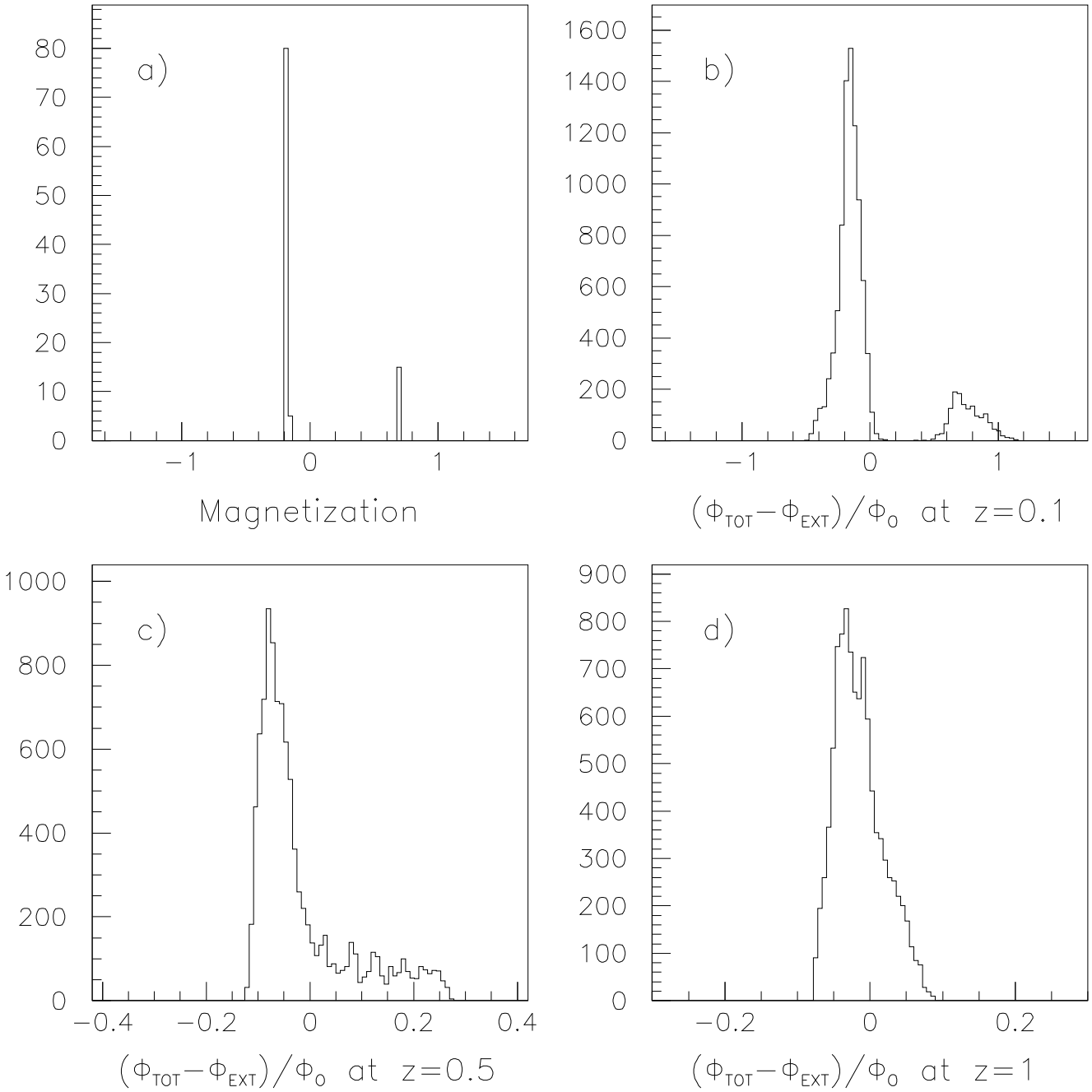
a)
b)
c)
d)
Magnetization
$(\Phi_{TOT}-\Phi_{EXT})/\Phi_0$ at z=0.1
$(\Phi_{TOT}-\Phi_{EXT})/\Phi_0$ at z=0.5
$(\Phi_{TOT}-\Phi_{EXT})/\Phi_0$ at z=1

Fig.6

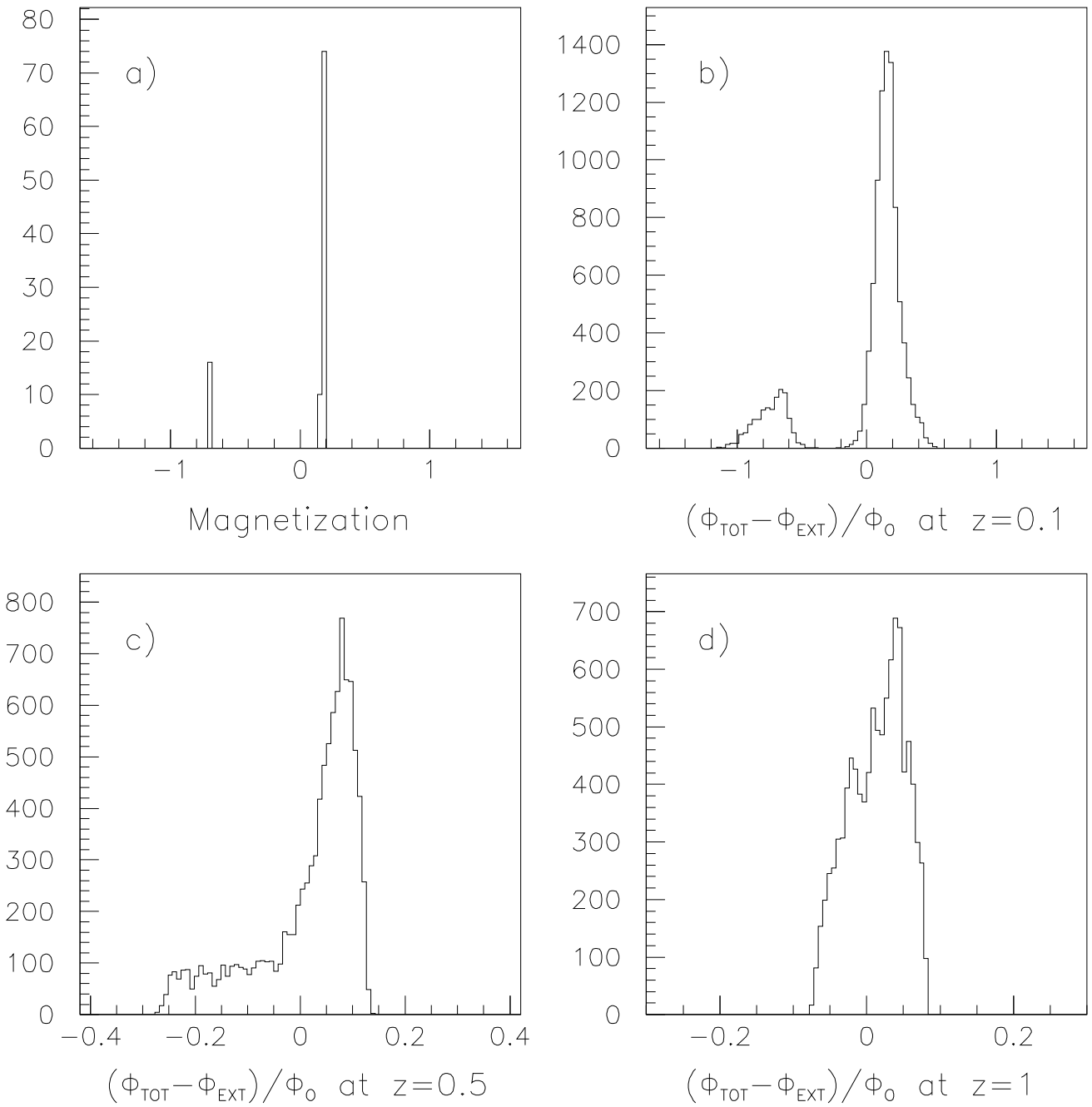
a)
b)
c)
d)
Magnetization
$(\Phi_{TOT}-\Phi_{EXT})/\Phi_0$ at z=0.1
$(\Phi_{TOT}-\Phi_{EXT})/\Phi_0$ at z=0.5
$(\Phi_{TOT}-\Phi_{EXT})/\Phi_0$ at z=1

Fig.7

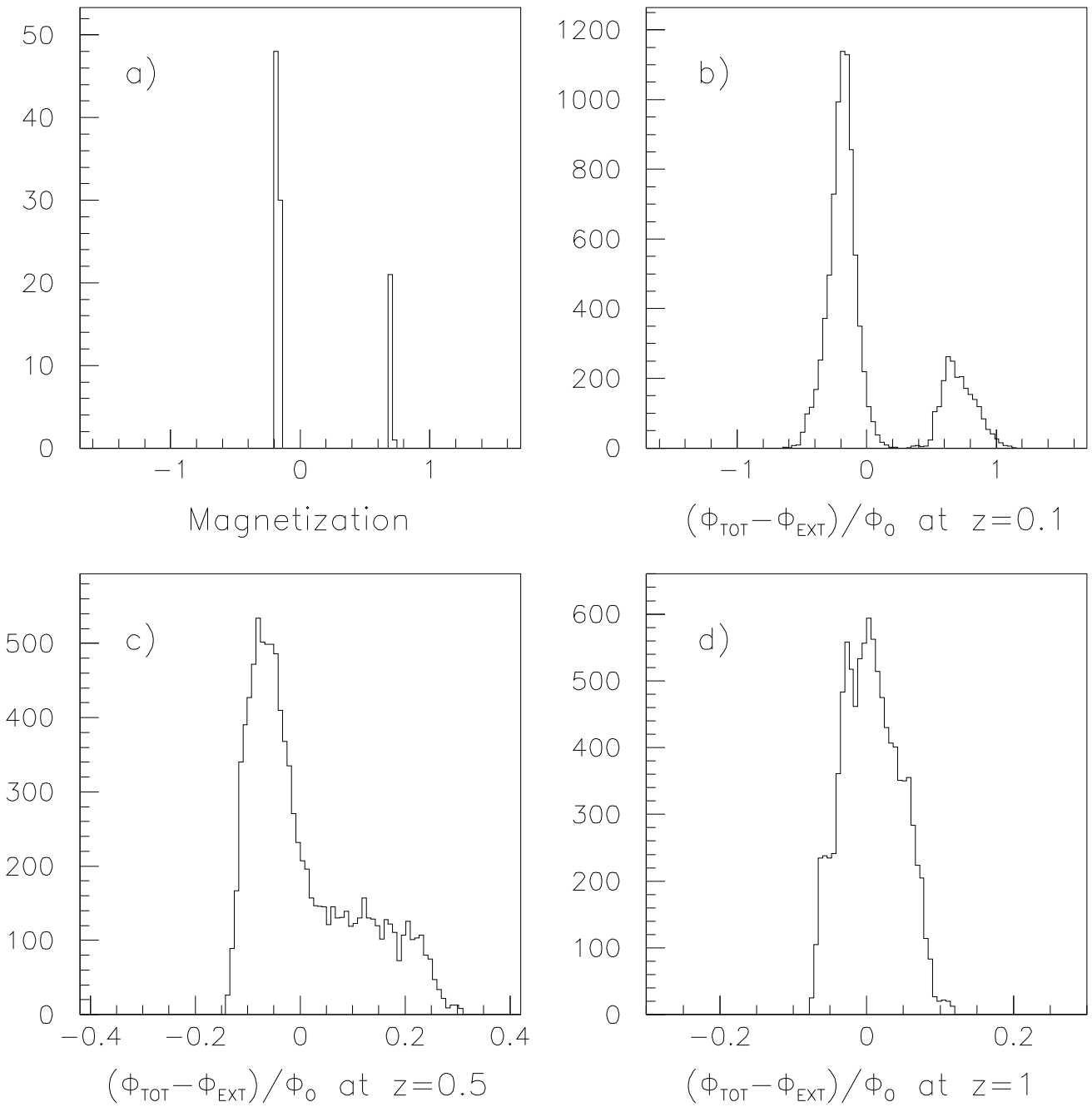
a)
b)
c)
d)
Magnetization
$(\Phi_{TOT}-\Phi_{EXT})/\Phi_0$ at z=0.1
$(\Phi_{TOT}-\Phi_{EXT})/\Phi_0$ at z=0.5
$(\Phi_{TOT}-\Phi_{EXT})/\Phi_0$ at z=1

Fig.8

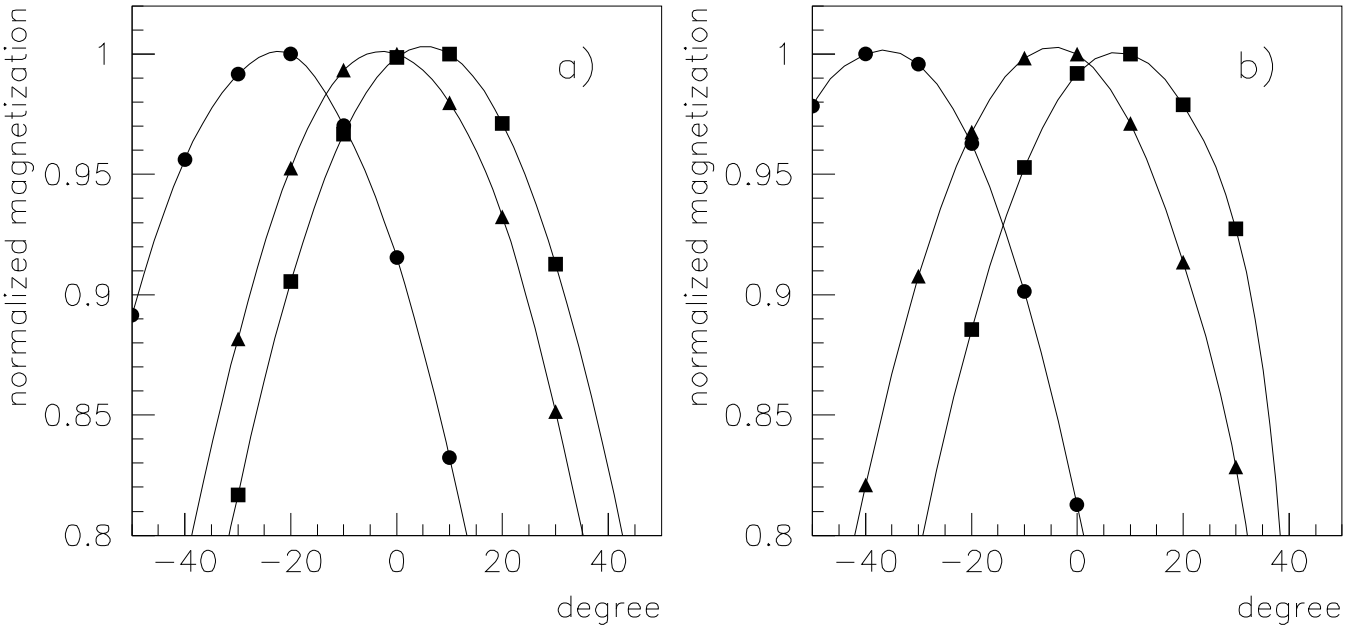
normalized magnetization
1
0.95
0.9
0.85
0.8
−40
−20
0
20
40
degree
a)
b)